Adiabatic microring modulators

Aleksandr Biberman,[1] Erman Timurdogan,[1] William A. Zortman,[2] Douglas C. Trotter,[2] and Michael R. Watts[1,*]

[1]*Research Laboratory of Electronics, Massachusetts Institute of Technology, 77 Massachusetts Avenue, Cambridge, Massachusetts 02139, USA*

[2]*Sandia National Laboratories, P. O. Box 5800, Albuquerque, New Mexico 87185, USA*

**mwatts@mit.edu*

Abstract: In this work, we demonstrate and experimentally characterize a new class of high-performance silicon photonic modulators—the adiabatic microring modulator. The adiabatic microring modulator utilizes a vertical PN junction and interior electrical contacts, leveraging all the advantages of previously-demonstrated microdisk modulators. However, this device also incorporates an adiabatic transition from the wide, multimode contact region, to a narrow, single-mode coupling region, eliminating unwanted spatial modes common to microdisks. As a result, the adiabatic microring modulator demonstrated in this work is the smallest microring modulator demonstrated to date, with a diameter of only 4 μm, yielding a 6.92-THz uncorrupted free spectral range. Here, we perform an experimental comparative analysis between silicon adiabatic microring modulators, silicon microdisk modulators, and a commercial lithium-niobate Mach-Zehnder modulator. We show that the silicon adiabatic microring modulator using partial doping is capable of operating at 12.5-Gb/s data rates and beyond. This device combines the best of all modulator designs, leveraging the depletion-based method to maximize the speed, utilizing the vertical-junction configuration to minimize the power consumption, employing a unique adiabatic design to eliminate higher-order modes, and using partial doping to reduce resistance, further enhancing the speed of the device.

OCIS codes: (250.3140) Integrated optoelectronic circuits; (250.4110) Modulators; (130.0250) Optoelectronics; (230.3120) Integrated optics devices.

References and links

1. D. A. B. Miller, "Device requirements for optical interconnects to silicon chips," Proc. IEEE **97**(7), 1166–1185 (2009).
2. A. Biberman, "Silicon photonic revolution through advanced integration," Future Fab Intl. **42**, 25–28 (2012).
3. A. Biberman and K. Bergman, "Optical interconnection networks for high-performance computing systems," Rep. Prog. Phys. **75**(4), 046402 (2012).
4. A. Liu, R. Jones, L. Liao, D. Samara-Rubio, D. Rubin, O. Cohen, R. Nicolaescu, and M. Paniccia, "A high-speed silicon optical modulator based on a metal-oxide-semiconductor capacitor," Nature **427**(6975), 615–618 (2004).
5. Q. Xu, B. Schmidt, S. Pradhan, and M. Lipson, "Micrometre-scale silicon electro-optic modulator," Nature **435**(7040), 325–327 (2005).
6. M. R. Watts, D. C. Trotter, R. W. Young, and A. L. Lentine, "Ultralow power silicon microdisk modulators and switches," Proc. International Conference on Group IV Photonics (GFP), WA2 (2008).
7. M. R. Watts, W. A. Zortman, D. C. Trotter, R. W. Young, and A. L. Lentine, "Vertical junction silicon microdisk modulators and switches," Opt. Express **19**(22), 21989–22003 (2011).
8. G. Li, X. Zheng, J. Yao, H. Thacker, I. Shubin, Y. Luo, K. Raj, J. E. Cunningham, and A. V. Krishnamoorthy, "25Gb/s 1V-driving CMOS ring modulator with integrated thermal tuning," Opt. Express **19**(21), 20435–20443 (2011).
9. W. A. Zortman, A. L. Lentine, D. C. Trotter, and M. R. Watts, "Low-voltage differentially-signaled modulators," Opt. Express **19**(27), 26017–26026 (2011).
10. M. R. Watts, "Adiabatic microring resonators," Opt. Lett. **35**(19), 3231–3233 (2010).
11. M. R. Watts, W. A. Zortman, D. C. Trotter, G. N. Nielson, D. L. Luck, and R. W. Young, "Adiabatic resonant microrings (ARMs) with directly integrated thermal microphotonics," Proc. Conference on Lasers and Electro-Optics (CLEO), CPDB10 (2009).
12. E. Timurdogan, M. Moresco, A. Biberman, J. Sun, W. A. Zortman, D. C. Trotter, and M. R. Watts, "Adiabatic resonant microring (ARM) modulator," Proc. Optical Interconnects Conference (OI Conference), TuC6 (2012).

#177942 - $15.00 USD Received 11 Oct 2012; revised 4 Dec 2012; accepted 10 Dec 2012; published 17 Dec 2012

13. A. Biberman, S. Manipatruni, N. Ophir, L. Chen, M. Lipson, and K. Bergman, "First demonstration of long-haul transmission using silicon microring modulators," Opt. Express **18**(15), 15544–15552 (2010).
14. W. A. Zortman, A. L. Lentine, M. R. Watts, and D. C. Trotter, "Power penalty measurement and frequency chirp extraction in silicon microdisk resonator modulators," Proc. Optical Fiber Communication Conference (OFC), OMI7 (2010).
15. P. Dong, S. Liao, D. Feng, H. Liang, D. Zheng, R. Shafiiha, C.-C. Kung, W. Qian, G. Li, X. Zheng, A. V. Krishnamoorthy, and M. Asghari, "Low V_{pp}, ultralow-energy, compact, high-speed silicon electro-optic modulator," Opt. Express **17**(25), 22484–22490 (2009).
16. P. Dong, S. Liao, H. Liang, W. Qian, X. Wang, R. Shafiiha, D. Feng, G. Li, X. Zheng, A. V. Krishnamoorthy, and M. Asghari, "High-speed and compact silicon modulator based on a racetrack resonator with a 1 V drive voltage," Opt. Lett. **35**(19), 3246–3248 (2010).
17. X. Xiao, H. Xu, X. Li, Y. Hu, K. Xiong, Z. Li, T. Chu, Y. Yu, and J. Yu, "25 Gbit/s silicon microring modulator based on misalignment-tolerant interleaved PN junctions," Opt. Express **20**(3), 2507–2515 (2012).
18. J. C. Rosenberg, W. M. J. Green, S. Assefa, D. M. Gill, T. Barwicz, M. Yang, S. M. Shank, and Y. A. Vlasov, "A 25 Gbps silicon microring modulator based on an interleaved junction," Opt. Express **20**(24), 26411–26423 (2012).
19. G. Li, X. Zheng, J. Yao, H. Thacker, I. Shubin, Y. Luo, K. Raj, J. E. Cunningham, and A. V. Krishnamoorthy, "25Gb/s 1V-driving CMOS ring modulator with integrated thermal tuning," Opt. Express **19**(21), 20435–20443 (2011).
20. G. Li, X. Zheng, H. Thacker, J. Yao, Y. Luo, I. Shubin, K. Raj, J. E. Cunningham, and A. V. Krishnamoorthy, "40 Gb/s thermally tunable CMOS ring modulator," Proc. International Conference on Group IV Photonics (GFP), 1–3 (2012).
21. Y. Hu, X. Xiao, H. Xu, X. Li, K. Xiong, Z. Li, T. Chu, Y. Yu, and J. Yu, "High-speed silicon modulator based on cascaded microring resonators," Opt. Express **20**(14), 15079–15085 (2012).
22. X. Xiao, X. Li, H. Xu, Y. Hu, K. Xiong, Z. Li, T. Chu, J. Yu, and Y. Yu, "44-Gb/s silicon microring modulators based on zigzag PN junctions," IEEE Photon. Technol. Lett. **24**(19), 1712–1714 (2012).
23. A. Biberman, M. J. Shaw, E. Timurdogan, J. B. Wright, and M. R. Watts, "Ultralow-loss silicon ring resonators," Opt. Lett. **37**(20), 4236–4238 (2012).
24. M. R. Watts, D. C. Trotter, and R. W. Young, "Maximally confined high-speed second-order silicon microdisk switches," Proc. Optical Fiber Communication Conference (OFC), PDP14 (2008).
25. A. Biberman, H. L. R. Lira, K. Padmaraju, N. Ophir, J. Chan, M. Lipson, and K. Bergman, "Broadband silicon photonic electrooptic switch for photonic interconnection networks," IEEE Photon. Technol. Lett. **23**(8), 504–506 (2011).
26. M. A. Popovíc, T. Barwicz, M. R. Watts, P. T. Rakich, L. Socci, E. P. Ippen, F. X. Kärtner, and H. I. Smith, "Multistage high-order microring-resonator add-drop filters," Opt. Lett. **31**(17), 2571–2573 (2006).
27. R. E. Camacho-Aguilera, Y. Cai, N. Patel, J. T. Bessette, M. Romagnoli, L. C. Kimerling, and J. Michel, "An electrically pumped germanium laser," Opt. Express **20**(10), 11316–11320 (2012).
28. D. Ahn, C. Y. Hong, J. Liu, W. Giziewicz, M. Beals, L. C. Kimerling, J. Michel, J. Chen, and F. X. Kärtner, "High performance, waveguide integrated Ge photodetectors," Opt. Express **15**(7), 3916–3921 (2007).
29. C. T. DeRose, D. C. Trotter, W. A. Zortman, A. L. Starbuck, M. Fisher, M. R. Watts, and P. S. Davids, "Ultra compact 45 GHz CMOS compatible Germanium waveguide photodiode with low dark current," Opt. Express **19**(25), 24897–24904 (2011).
30. M. R. Watts and H. A. Haus, "Integrated mode-evolution-based polarization rotators," Opt. Lett. **30**(2), 138–140 (2005).
31. M. R. Watts, H. A. Haus, and E. P. Ippen, "Integrated mode-evolution-based polarization splitter," Opt. Lett. **30**(9), 967–969 (2005).
32. T. Barwicz, M. R. Watts, M. A. Popovic, P. T. Rakich, L. Socci, F. X. Kärtner, E. P. Ippen, and H. I. Smith, "Polarization-transparent microphotonic devices in the strong confinement limit," Nat. Photonics **1**(1), 57–60 (2007).
33. D. Dai and J. E. Bowers, "Novel concept for ultracompact polarization splitter-rotator based on silicon nanowires," Opt. Express **19**(11), 10940–10949 (2011).
34. A. R. Johnson, Y. Okawachi, J. S. Levy, J. Cardenas, K. Saha, M. Lipson, and A. L. Gaeta, "Chip-based frequency combs with sub-100 GHz repetition rates," Opt. Lett. **37**(5), 875–877 (2012).
35. W. Mathlouthi, H. Rong, and M. Paniccia, "Characterization of efficient wavelength conversion by four-wave mixing in sub-micron silicon waveguides," Opt. Express **16**(21), 16735–16745 (2008).
36. X. Zheng, F. Y. Liu, J. Lexau, D. Patil, G. Li, Y. Luo, H. D. Thacker, I. Shubin, J. Yao, K. Raj, R. Ho, J. E. Cunningham, and A. V. Krishnamoorthy, "Ultralow power 80 Gb/s arrayed CMOS silicon photonic transceivers for WDM optical links," J. Lightwave Technol. **30**(4), 641–650 (2012).
37. I. A. Young, E. Mohammed, J. T. S. Liao, A. M. Kern, S. Palermo, B. A. Block, M. R. Reshotko, and P. L. D. Chang, "Optical I/O technology for tera-scale computing," IEEE J. Solid-state Circuits **45**(1), 235–248 (2010).

1. Introduction

Compact, high-speed, low-power, and CMOS-compatible silicon photonic devices and systems are being widely considered for achieving aggressive performance goals in future computation and communication systems [1–3]. The silicon photonic toolbox already comprises modulators [4–22], waveguides [23], switches [24,25], filters [26], lasers [27],

#177942 - $15.00 USD Received 11 Oct 2012; revised 4 Dec 2012; accepted 10 Dec 2012; published 17 Dec 2012

photodetectors [28,29], polarization-manipulating devices [30–33], and nonlinear devices [34,35]. Combining these components, compact, low-cost, wavelength-division-multiplexed (WDM) communication links may be formed [36,37]. Silicon photonic modulators represent the key components for encoding data from the electrical domain to the optical domain [4–22]. Silicon microring modulators, first demonstrated in the injection-based lateral-junction configuration by Q. Xu *et al.* [5], have been primarily considered for these applications because they are compact, high-speed, low-power, and are capable of enabling WDM systems with many wavelength channels.

Depletion-based devices improve on these early injection-based device designs, enabling efficient high-speed operation of silicon microring and microdisk modulators. Recent work has yielded depletion-based modulators leveraging lateral-junction configurations capable of operating beyond 25 [17–19], and even 40 Gb/s [20–22]. Methods to interleave PN junctions have been utilized to increase the electro-optic efficiency by enhancing the carrier-light overlap, which reduces the voltage-length product $V_\pi L_\pi$, achieving 25-Gb/s operation of a 30-μm-radius device with 4.5-dB extinction ratio at 2-V driving voltage [17], and 25-Gb/s operation of a 250-μm-circumference device with about 3.6-dB extinction ratio at 1.6-V driving voltage and 41-fJ/bit power consumption [18]. Another demonstration has achieved 25-Gb/s operation of a 7.5-μm-radius device with about 5-dB extinction ratio at 1-V driving voltage and about 7-fJ/bit power consumption [19]. By reducing the radius of the latter device to 5 μm, reducing the junction capacitance and the RC time constant, a similar device was demonstrated to operate at 40 (44) Gb/s, with 7- (2.3-) dB extinction ratios at 2-V driving voltages [20]. Leveraging PN-junction-interleaved cascaded microring resonators, 40-Gb/s operation was demonstrated with a 20-μm-radius device with 3.9-dB extinction ratio at 5-V driving voltage [21]. Lastly, a method to zigzag the PN junction has been employed to achieve 44-Gb/s operation with 3.01-dB extinction ratio at 3-V driving voltage [22].

Depletion-based devices leveraging vertical-junction configurations provide the added advantage to the drive voltage, power consumption, size, and speed [7]. The vertical junction naturally maximizes the overlap of the depletion region with the optical mode, reducing the drive voltage and power consumption. It also enables direct electrical contacts to be made at the interior of the silicon microdisk or microring resonator, forming a hard outer wall that minimizes radiation, resulting in a significant size reduction of the device. This reduction in size also reduces the capacitance, reducing the RC time constant and increasing the speed. For example, depletion-based vertical-junction silicon microdisk modulators have enabled 12.5-Gb/s modulation of a 1.75-μm-radius device with 3.2-dB extinction ratio at 1-V driving voltage and 3-fJ/bit power consumption [7]. This device occupies less than one-tenth the area of traditional microring modulators, and maintains entirely-interior electrical contacts.

However, one major limitation of microdisk resonators is that they support higher-order spatial modes that corrupt the free spectral range (FSR) by introducing undesired resonances. To combat this, several demonstrations have utilized adiabatic microring resonators, which leverage single-mode coupling regions and multimode contact regions to achieve single-mode operation [10–12]. These devices preserve all the benefits of microdisk resonators, with the added advantage of enabling uncorrupted FSRs [10]. One demonstration has directly integrated heaters within adiabatic microring resonators, achieving 4.4-μW/GHz power

#177942 - $15.00 USD Received 11 Oct 2012; revised 4 Dec 2012; accepted 10 Dec 2012; published 17 Dec 2012

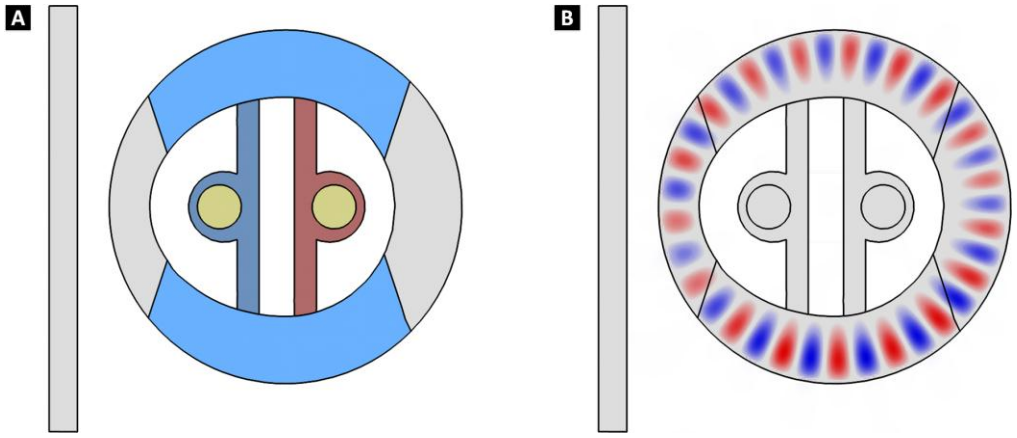

Fig. 1. (a) Top-view schematic of the silicon adiabatic microring modulator using partial doping, utilizing a single-mode coupling region and a multimode contact region of the microring resonator. (b) 3D finite-difference time-domain (FDTD) simulation overlaying the schematic, showing that only the fundamental radial mode is excited.

dissipation and 1-μs thermal tuning speed of a second-order filter [11]. Another demonstration has presented preliminary results of a depletion-based vertical-junction adiabatic microring modulator, with an uncorrupted 6.9-THz FSR, achieving 12-Gb/s operation of a 2-μm-radius device with about 7.3-dB extinction ratio at 2.4-V driving voltage [12].

In this work, we present the design and first quantitative results of the adiabatic microring modulator. We show that the partial doping modulator configuration reduces the resistance and enhances the speed of the device. We perform a detailed comparative analysis between four silicon photonic modulators, including silicon microdisk modulators and silicon adiabatic microring modulators, with full and partial doping configurations, and as well as the commercial lithium niobate modulator. Our high-speed bit-error-rate and power penalty characterizations show that the partial doping causes a reduction in relative power penalty for both silicon microdisk and adiabatic microring modulators, enabling feasible operation of both at 12.5-Gb/s data rates and beyond.

2. Adiabatic microring resonator

The design of the adiabatic microring resonator consists of a single-mode coupling region and multimode contact region. The basic structure is depicted in Fig. 1(a). In the coupling region, the microring waveguide has a width of 460 nm, and the bus waveguide has a width of 320 nm, both kept narrow to ensure single-mode operation. The coupling gap was then chosen to be 360 nm, and designed to ensure critical coupling on resonance. The microring waveguide is adiabatically widened with a half ellipse inner radius to enable electrical contact where there is essentially no optical field. At the widest point, the microring waveguide reaches a width of 760 nm, and the microring is clearly multimode. However, the single-mode coupling region and adiabatic transition to the multimode contact region ensure that only the fundamental radial mode is excited. A 3D finite-difference time-domain (FDTD) simulation highlights this point in Fig. 1(b). Design and fabrication of similar adiabatic microrings has previously been demonstrated both numerically [10] and experimentally [11,12], respectively.

The modulators in this work were fabricated at the CMOS fabrication facility of Sandia National Laboratories, on a 240-nm-thick silicon-on-insulator (SOI) platform, with a 1-μm buried oxide (BOX) layer, using 248-nm deep ultraviolet (DUV) lithography. All of these modulators incorporate 400-nm-diameter tungsten contacts that connect electrical probes to the device. The anode (cathode) contact connects to the 10^{20} P + type (N + type) doped silicon using titanium silicide at the interface, which then connects to the 2×10^{18} P type (N type)

#177942 - $15.00 USD Received 11 Oct 2012; revised 4 Dec 2012; accepted 10 Dec 2012; published 17 Dec 2012

doped silicon. The P + and N + type doped silicon regions act as ohmic contacts to the diodes. The P and N type doped silicon layers are each approximately 100-nm thick, which form

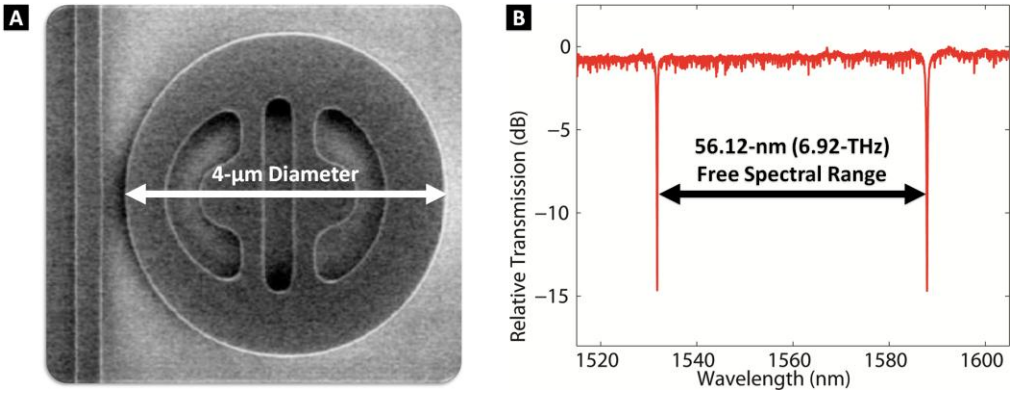

Fig. 2. (a) Top-view scanning-electron-microscope (SEM) image of the silicon adiabatic microring modulator, which comprises a 4-μm-diameter microring resonator, in the depletion-based vertical-junction configuration to minimize the power consumption. (b) Spectral response of this device, showing two consecutive resonances with an uncorrupted 56.12-nm (6.92-THz) free spectral range (FSR).

depletion regions at their vertical junctions. The P + type (N + type) doped silicon is 100-nm (240-nm) thick to connect to the P type (N type) doped silicon on top (bottom). A scanning-electron-microscope (SEM) image of the fabricated silicon layer is shown in Fig. 2(a).

Adiabatic microring resonators are designed to eliminate the coupling of higher-order TE optical modes to achieve uncorrupted FSRs and low insertion losses. Other suppression methods, such as patterning highly-doped regions in the center of the microdisk, would lower the quality (Q) factor of the second-order mode, but would not eliminate it. This would lead to a high insertion loss, as well as crosstalk for other wavelength channels in a WDM scheme. In order to achieve a low-enough Q factor for the second order mode, the first mode would also experience additional insertion loss, which would increase the optical bandwidth (decrease the Q factor), and decrease the dynamic extinction ratio for the same frequency shift.

The structures are first tested passively using a tunable laser source, and the results are presented in Fig. 2(b). As also predicted by simulation [10], the adiabatic microring achieves a wide, 6.92-THz FSR, uncorrupted by higher-order spatial modes.

3. Silicon photonic modulators

In this work, we quantify the electro-optic performance of adiabatic microring modulators, and perform comparisons with silicon microdisk modulators, as well as with a commercial lithium niobate modulator. The four types of silicon photonic modulators are depicted in Fig. 3. We first demonstrate and experimentally characterize silicon adiabatic microring modulators, shown in Fig. 2(a) and Figs. 3(c)–3(d). Furthermore, we perform a comparative analysis with the silicon microdisk modulators, depicted in Figs. 3(a)–3(b), as well as a commercial lithium-niobate ($LiNbO_3$) Mach-Zehnder modulator. The presented silicon adiabatic microring modulator using partial doping: (1) leverages the depletion-based method to maximize the speed; (2) utilizes the vertical-junction configuration, which maximizes the overlap of the depletion region with the optical mode, minimizing the power consumption; (3) employs a unique adiabatic design that eliminates higher-order modes that are present in the silicon microdisk modulator, as shown in Fig. 1(b); (4) is partially doped, as depicted in Fig. 3(d), reducing the resistance and enhancing the speed of the device. We demonstrate that the silicon adiabatic microring modulator using partial doping has comparable performance to the silicon microdisk modulator using partial doping, and that both devices are capable of feasibly operating at 12.5-Gb/s data rates and beyond.

#177942 - $15.00 USD Received 11 Oct 2012; revised 4 Dec 2012; accepted 10 Dec 2012; published 17 Dec 2012

4. Experimental setup

The experimental setup to characterize the silicon photonic modulators in this work, depicted in Fig. 4(a), consists of a tunable laser (TL) source, which transmits a CW lightwave into the

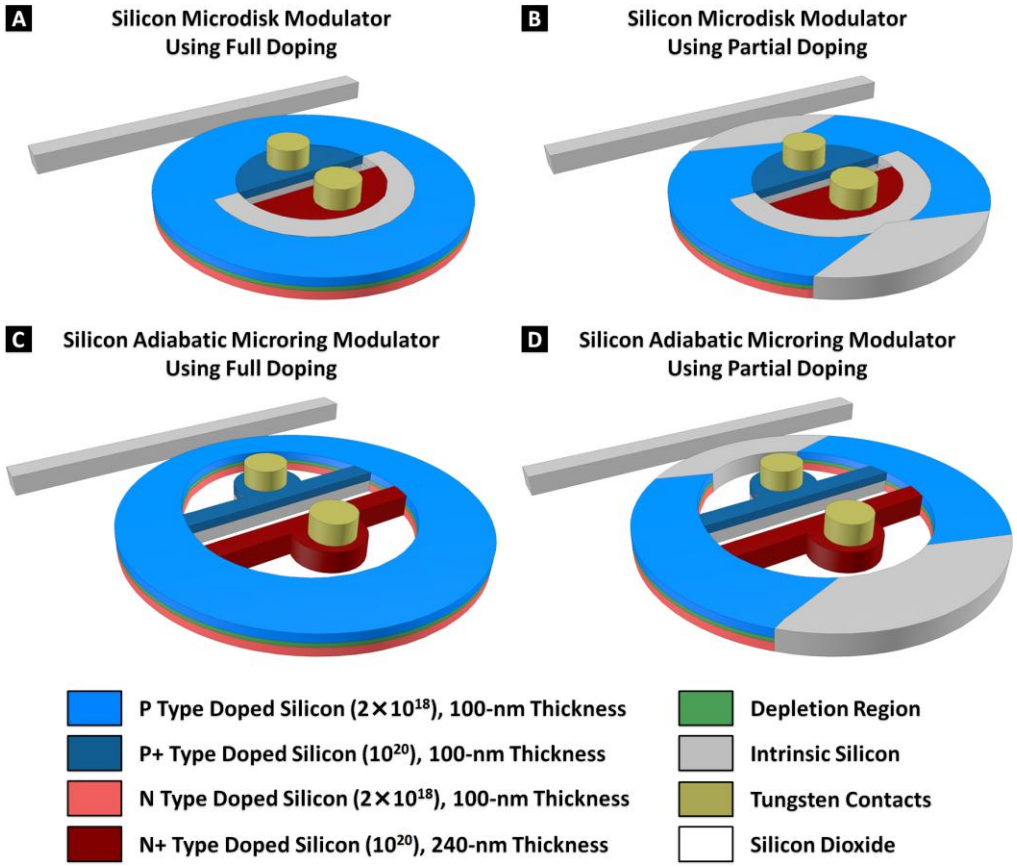

Fig. 3. Four types of silicon photonic modulators, including silicon microdisk modulators and silicon adiabatic microring modulators, with full and partial doping configurations. These depletion-based modulators all employ the vertical-junction configuration to minimize the power consumption.

silicon chip using lensed fibers. Once on chip, the lightwave is then spectrally aligned to a resonance of the microdisk or microring of the modulator, which is about 1574 or 1594 nm, respectively. Induced by the plasma-dispersion effect, this resonance is then spectrally shifted back and forth when we toggle an electrical bias, which toggles the depth of the depletion region through the vertical PN diode. In this work, the electrical bias is a non-return-to-zero (NRZ) on-off-keyed (OOK) signal, generated using a pattern generator (PG), encoded with a 2^{31}–1 pseudo-random bit sequence (PRBS). This signal is then amplified and offset to produce a 2.5-V_{pp} electrical signal with a –1-V voltage bias; the voltage rails are at 0.25 and –2.25 V. The electrical signal is then transmitted into the chip using 50-Ω-terminated electrical probes. Because the modulators in this work employ the depletion-based configuration, which does not suffer from electrical carrier lifetime limitations, there is no need to supplement the driving signal with pre-emphasis at higher data rates.

The lightwave is spectrally aligned to the resonance such that when the voltage is at 0.25 V, the lightwave couples to the microdisk or microring and inhibits propagation out of the chip, representing a logical *0* state. When the voltage is at –2.25 V, the lightwave bypasses the microdisk or microring and propagates out of the chip, representing a logical *1* state.

#177942 - $15.00 USD Received 11 Oct 2012; revised 4 Dec 2012; accepted 10 Dec 2012; published 17 Dec 2012

Therefore, by modulating the electrical signal with high-speed data, we encode this data onto the optical domain. Off chip, the high-speed optical signal then passes through an erbium-doped fiber amplifier (EDFA), a tunable grating filter (λ) with a 1-nm 3-dB bandwidth, and a variable optical attenuator (VOA). The signal is then received using a high-speed PIN

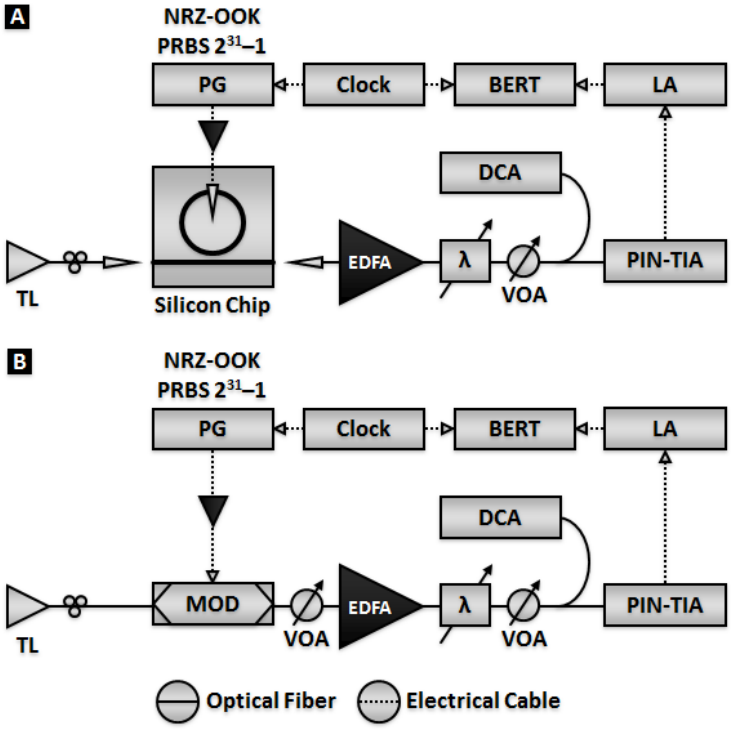

Fig. 4. Experimental setup diagrams for characterizing the performance of the (a) four silicon photonic modulators, as well as (b) the commercial lithium niobate modulator. Temporal responses of the high-speed optical data were measured at 2.5-, 5-, 7.5-, 10-, and 12.5-Gb/s data rates, and bit-error-rate (BER) characterizations were performed at 5, 7.5, and 10 Gb/s.

photodiode and transimpedance amplifier (PIN-TIA) receiver followed by a limiting amplifier (LA), and is evaluated using a bit-error-rate (BER) tester (BERT). Both the PG and the BERT are synchronized to the same clock. Using a power tap, a digital communications analyzer (DCA) is used to examine the temporal response of the signal before the receiver. Polarization controllers (PCs) are also used throughout the setup, configured for TE operation. The total fiber-to-fiber insertion loss is about 17 dB for all of the devices; there is about –8-dBm (–19-dBm) average optical power ingressing into the modulator (EDFA), in every configuration. In the experimental setup comparing the performance of the silicon photonic modulators to a commercial lithium niobate Mach-Zehnder modulator, as depicted in Fig. 4(b), we replace the silicon chip with the commercial modulator. The lithium niobate modulator has a 35-GHz 3-dB bandwidth, and is driven with an AC-coupled 5.5-V_{pp} electrical signal. For this modulator, there is also about –8-dBm average optical power ingressing into the modulator, and a VOA is used right after the modulator to ensure that –19-dBm average optical power is ingressing into the EDFA. During these experiments, there was no observable resonance wavelength dependence on the data rate of the device or the PRBS pattern length.

5. Spectral characterization

We perform a spectral characterization of all the silicon photonic modulators to quantify the resonance spectral shift associated with varying applied DC voltages at the modulator diode junction, comparing the silicon adiabatic microring modulators to the silicon microdisk

#177942 - $15.00 USD Received 11 Oct 2012; revised 4 Dec 2012; accepted 10 Dec 2012; published 17 Dec 2012

modulators. For all of these devices, as shown in Fig. 5 and Fig. 6, we observe larger spectral blue (red) shifts as we apply larger positive (negative) voltages. We note that spectral blue shifts induced by positive voltages follow an exponential trend, and become especially significant above the threshold voltage of about 0.7 V. Spectral red shifts induced by negative voltages follow more of a linear trend, and are less dramatic even down to –3 V. Moreover,

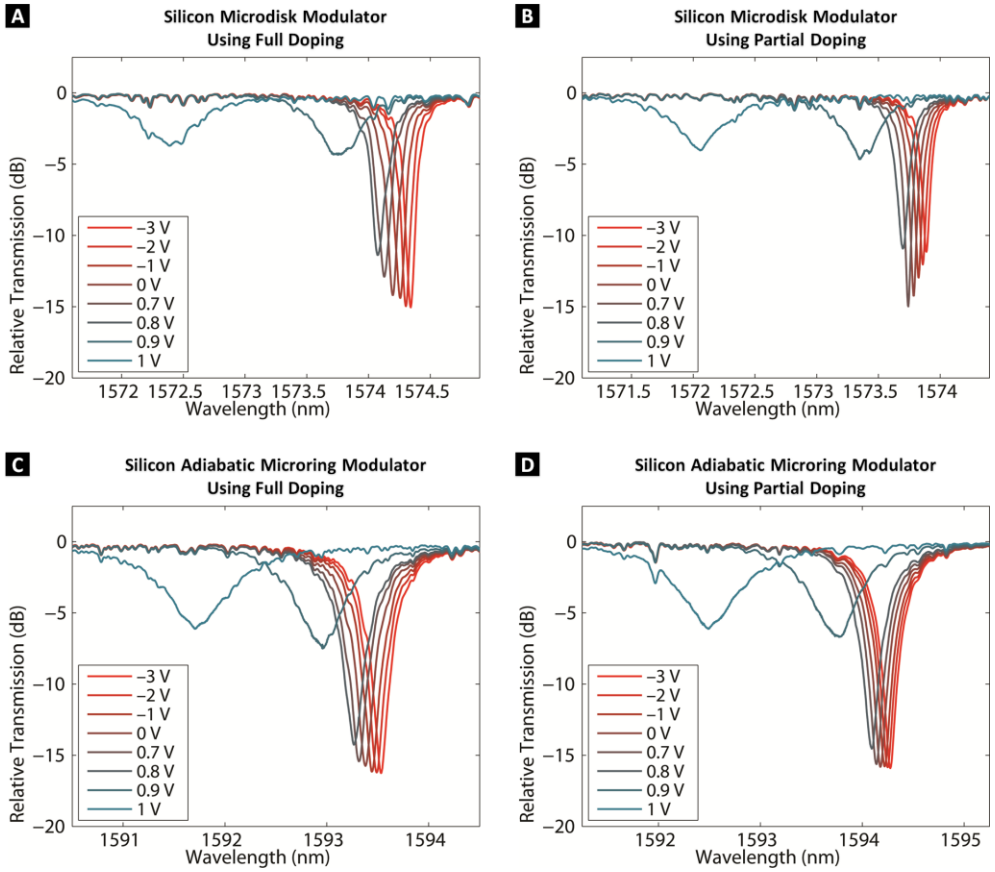

Fig. 5. Experimentally-measured resonance spectral shifts, induced by varying applied DC voltages at the modulator diode junction. This measurement, taken with –10 dBm of average optical power injected at the input of the silicon chip, characterizes four silicon photonic modulators, including silicon microdisk modulators and silicon adiabatic microring modulators, with full and partial doping configurations.

we see in Fig. 6 that the resonance frequency shift of all of the characterized silicon photonic modulators does not change significantly between devices. Therefore, the static resonance frequency shift as a function of applied modulator diode junction voltage does not have a dependency on whether we are using the silicon adiabatic microring modulators over silicon microdisk modulators, or partial doping over full doping. Furthermore, we see that both types of silicon microdisk modulators have similar resonance depths and static extinction ratios (Figs. 5(a)–5(b)), and both types of silicon adiabatic microring modulators also follow this trend (Figs. 5(c)–5(d)). However, the silicon microdisk modulators have smaller resonance depths, but larger static extinction ratios, compared to the silicon adiabatic microring modulators. The larger static extinction ratios are expected to yield larger dynamic extinction ratios during high-speed characterization, which will also influence the performance of these devices.

The measured full width at half maximum (FWHM) is 28.94 (20.82) and 65.46 (57.32) GHz, for the silicon microdisk modulator using full (partial) doping and silicon adiabatic

#177942 - $15.00 USD Received 11 Oct 2012; revised 4 Dec 2012; accepted 10 Dec 2012; published 17 Dec 2012

microring modulator using full (partial) doping, respectively. For the same devices, the measured loaded Q factor is 6581 (9149) and 2874 (3281), respectively. For the partially-doped devices, we expect that the internal Q factors (not the loaded Q factors) are double that of the fully-doped devices. The measured loaded Q factors have a dependence on the internal Q factor, as well as the coupling Q factor. The magnitude of the coupling Q factors, which could be different for the two types of devices, determines the magnitude of the impact that the internal Q factor has on each device.

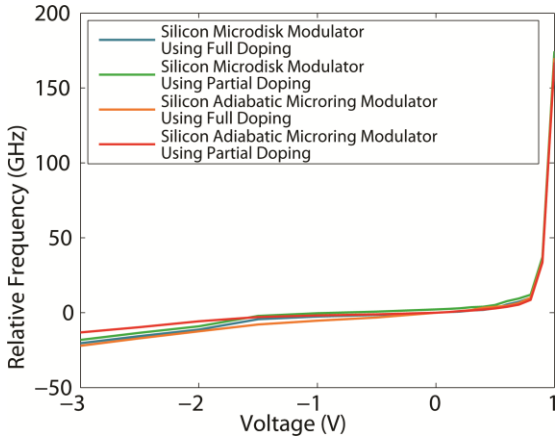

Fig. 6. Experimentally-measured resonance frequency shifts, induced by varying applied DC voltages at the modulator diode junction, for four silicon photonic modulators.

6. High-speed temporal characterization

Using the aforementioned experimental setup, depicted in Fig. 4(a), we first characterize all four silicon photonic modulators for a quantitative comparison. We drive the silicon microdisk modulator using full doping (Fig. 3(a)), at data rates between 2.5 and 12.5 Gb/s, and record the corresponding eye diagrams of the optical signal egressing from the silicon chip, as shown in Fig. 7(a). We observe excellent noise performance and extinction ratios for data rates up to 7.5 Gb/s. At 10 Gb/s, we begin to observe some added noise in the optical signal, corresponding to its speed limitation; at 12.5 Gb/s, we observe that this optical signal becomes even more constrained by this noise. For a direct comparison, we record similar eye diagrams for a silicon microdisk modulator using partial doping (Fig. 3(b)), at the same data rates. For this partially-doped modulator, for data rates up to 7.5 Gb/s, we observe a similar noise performance but slightly-lower extinction ratios compared to its fully-doped modulator counterpart. At 10 Gb/s, we observe better noise performance using the partially-doped modulator; this discrepancy becomes even more apparent as we drive the modulator at 12.5 Gb/s. We observe here that the silicon microdisk modulator using partial doping has a comparable performance at lower data rates to the silicon microdisk modulator using full doping, and much better performance at higher data rates—the partially-doped method enables this modulator to be feasible at 12.5-Gb/s data rates and beyond.

We then similarly characterize the silicon adiabatic modulator using full doping (Fig. 3(c)), between 2.5- and 12.5-Gb/s data rates, as shown in Fig. 7(c). Here, we see good noise performance up to 5 Gb/s, with slower rise and fall times compared to the silicon microdisk modulator. This speed limitation becomes more apparent at higher data rates. At 7.5 and 10 Gb/s, we observe an increasing degradation of the optical signal, and at 12.5 Gb/s, the eye diagram becomes too distorted to distinguish the bits of the pattern. However, using the silicon adiabatic microring modulator using partial doping (Fig. 3(a)), we observe a dramatic improvement in the optical signal integrity, as shown in Fig. 7(d), compared to its fully-doped modulator counterpart. In fact, we observe noise performance comparable to the best silicon microdisk modulator, shown in Fig. 7(b), at data rates up to 10 Gb/s. Furthermore, the partial

#177942 - $15.00 USD Received 11 Oct 2012; revised 4 Dec 2012; accepted 10 Dec 2012; published 17 Dec 2012

doping of the silicon adiabatic microring modulator also enables it to be feasible at 12.5-Gb/s data rates and beyond. Using the experimental setup depicted in Fig. 4(b), we then perform a similar characterization of the commercial lithium niobate Mach-Zehnder modulator, as shown in Fig. 7(e), for the baseline back-to-back measurement. As expected, the eye diagram for this device remains open as we sweep the data rate from 2.5 to 12.5 Gb/s.

Furthermore, we measure the dynamic extinction ratio and insertion loss for each modulator at every data rate between 2.5 and 12.5 Gb/s. The extinction ratio is defined as the ratio between the one and the zero of the optical signal, relative to the true zero; the true zero

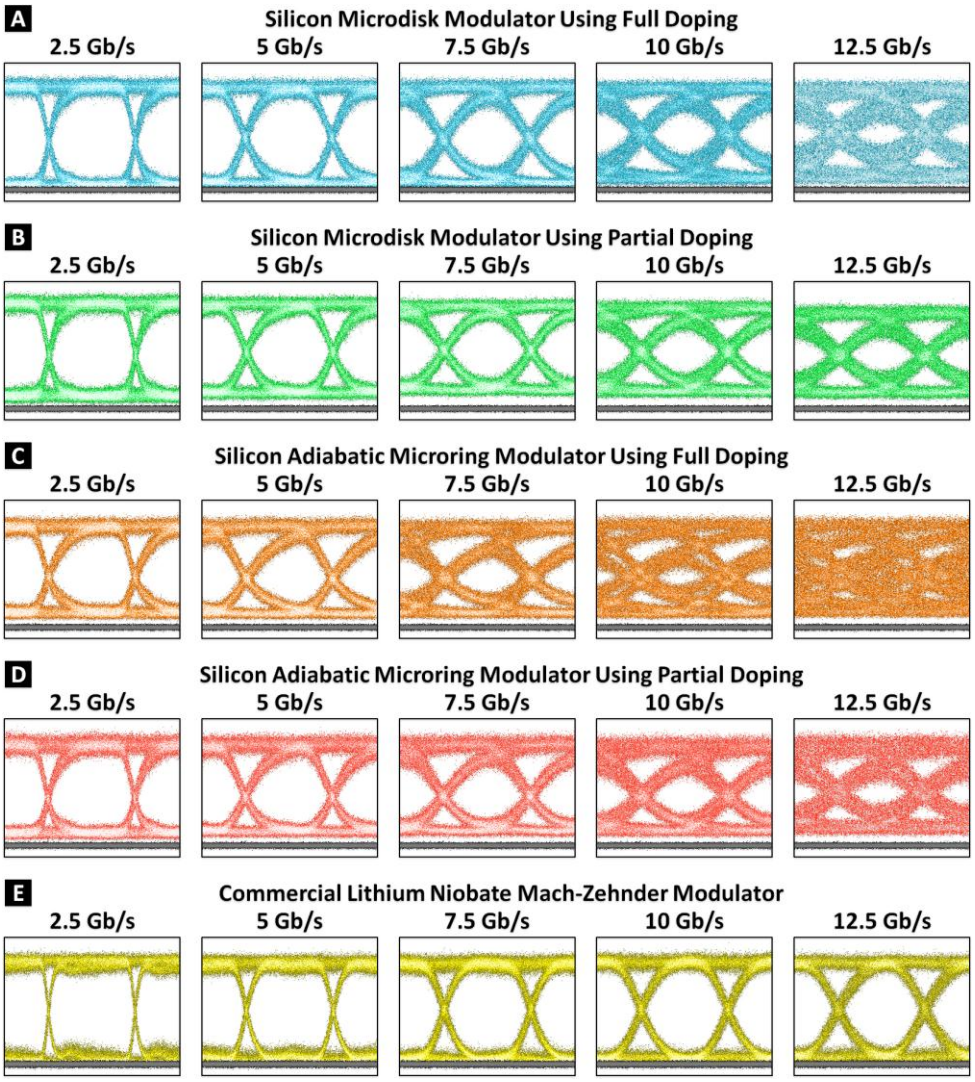

Fig. 7. Experimentally-measured optical eye diagrams egressing from the (a–d) four silicon photonic modulators, including silicon microdisk modulators and silicon adiabatic microring modulators, with full and partial doping configurations, and (e) the commercial lithium niobate modulator, for 2.5-, 5-, 7.5-, 10-, and 12.5-Gb/s data rates. The eye diagrams are overlaid with the true zero corresponding to each configuration.

is recorded using the same experimental setup depicted in Fig. 4(a), with the laser turned off, and is overlaid in Fig. 7 for each configuration. The insertion loss is defined as the ratio between the true one and the one of the optical signal, relative to the true zero; the true one is

#177942 - $15.00 USD Received 11 Oct 2012; revised 4 Dec 2012; accepted 10 Dec 2012; published 17 Dec 2012

recorded using the same experimental setup depicted in Fig. 4(a), and tuning up the wavelength of the ingressing CW lightwave 3 nm, along with the tunable grating filter, to spectrally bypass the resonance of the modulator. With a constant electrical driving signal that induces a finite resonance shift, it is possible to optimize the extinction ratio and insertion loss, trading off one of these parameters for the other. For example, operating closer to the center of the resonance optimizes the extinction ratio at the cost of the insertion loss. Shifting away from the resonance produces a converse effect. Since our experimental setup is not limited by insertion loss, for each configuration we optimize and measure the extinction ratio by operating closer to the center of the resonance. In this same state, we then also measure the insertion loss for each configuration. These results are summarized in Fig. 9.

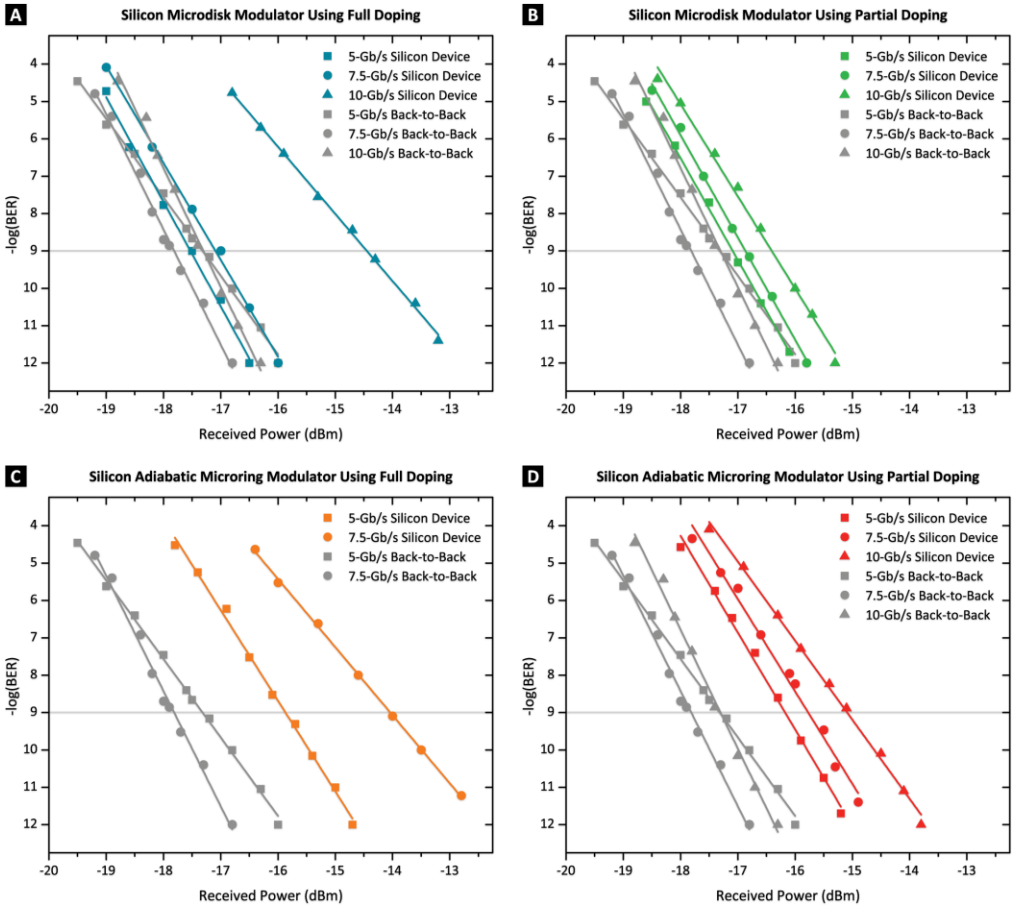

Fig. 8. Experimentally-measured bit-error-rate curves for four silicon photonic modulators, including silicon microdisk modulators and silicon adiabatic microring modulators, with full and partial doping configurations, and the commercial lithium niobate modulator, for 2.5-, 5-, 7.5-, 10-, and 12.5-Gb/s data rates. The bit-error-rate curves for the commercial lithium niobate modulator are set as the back-to-back cases for the silicon photonic modulator curves, producing a comparative power penalty between the two types of technologies in each configuration.

7. High-speed bit-error-rate and power penalty characterizations

Using the experimental setups described in Fig. 4, we then perform BER and power penalty characterizations for every type of silicon photonic modulator (Fig. 8). We first record the BER curves for the silicon photonic modulators operating at 5-, 7.5-, and 10-Gb/s data rates, which are shown in Fig. 8. For every shown BER curve, we also verify error-free operation,

#177942 - $15.00 USD Received 11 Oct 2012; revised 4 Dec 2012; accepted 10 Dec 2012; published 17 Dec 2012

which is defined as being capable of achieving BERs below 10^{-12}. We then record similar BER curves for the commercial lithium niobate modulator, operating at the same data rates, and plot these as back-to-back curves for the silicon photonic modulators (Fig. 8). This way, the resulting power penalty is defined as the relative signal integrity of each silicon photonic modulator, compared to the commercial lithium niobate modulator.

By setting the commercial lithium niobate modulator as the back-to-back cases for the silicon photonic modulators, we measure the resulting power penalty for every configuration. This measured power penalty is summarized in Fig. 9. For the silicon microdisk modulator using full doping, we observe a small negative power penalty of –0.22 dB, while operating at 5 Gb/s—at this data rate, this silicon photonic modulator has a superior signal integrity

Modulator Type	Data Rate	Extinction Ratio (dB)	Insertion Loss (dB)	Power Penalty (dB)
Silicon Microdisk Modulator Using Full Doping	2.5	14.94	1.92	–
	5	13.13	1.86	–0.22
	7.5	11.90	2.45	0.72
	10	9.84	2.25	2.85
	12.5	9.15	2.59	–
Silicon Microdisk Modulator Using Partial Doping	2.5	9.17	0.14	–
	5	8.16	0.19	0.20
	7.5	7.28	0.24	0.94
	10	7.42	0.24	0.89
	12.5	7.76	0.45	–
Silicon Adiabatic Microring Modulator Using Full Doping	2.5	8.52	0.70	–
	5	8.69	1.16	1.44
	7.5	7.93	1.43	3.77
	10	8.20	1.60	–
	12.5	7.73	1.66	–
Silicon Adiabatic Microring Modulator Using Partial Doping	2.5	9.03	1.86	–
	5	8.67	1.99	1.12
	7.5	8.15	2.59	2.05
	10	8.21	2.25	2.20
	12.5	7.34	2.59	–
Commercial Lithium Niobate Mach-Zehnder Modulator	2.5	14.24	4.00	–
	5	13.59	4.00	–
	7.5	12.67	4.00	–
	10	11.56	4.00	–
	12.5	11.49	4.00	–

Fig. 9. Table summarizing the experimentally-measured performance of four silicon photonic modulators, including silicon microdisk modulators and silicon adiabatic microring modulators, with full and partial doping configurations, and the commercial lithium niobate modulator, for 2.5-, 5-, 7.5-, 10-, and 12.5-Gb/s data rates. The measured power penalty of the silicon photonic modulators is in reference to the measured performance of the commercial lithium niobate modulator.

compared to its commercial counterpart. As we then modulate at 7.5 and 10 Gb/s, we observe that this power penalty turns positive and increases sharply to 0.72 and 2.85 dB, respectively. For the silicon microdisk modulator using partial doping, we observe a small positive power penalty of 0.20 and 0.94 dB, at the data rate of 5 and 7.5 Gb/s, respectively. At these lower data rates, the fully-doped version of the silicon photonic modulator outperforms the partially-doped version. However, as we modulate at 10 Gb/s, the power penalty for the partially-doped modulator is 0.89 dB, representing almost 2 dB of improvement over the fully-doped version.

For the silicon adiabatic microring modulator using full doping, we observe a moderate positive power penalty of 1.44 and 3.77 dB, at the data rate of 5 and 7.5 Gb/s, respectively. As

#177942 - $15.00 USD Received 11 Oct 2012; revised 4 Dec 2012; accepted 10 Dec 2012; published 17 Dec 2012

we then modulate at 10 Gb/s, the signal degradation is so large for this device that it is no longer capable of achieving error-free operation. However, the silicon adiabatic microring modulator using partial doping achieves a moderate positive power penalty of 1.12, 2.05, and 2.20 dB, for 5, 7.5, and 10 Gb/s. This partially-doped version of the modulator outperforms the fully-doped modulator at every data rate, and is capable of achieving error-free operation at least up to 10 Gb/s.

8. Conclusion

In this work, we demonstrate and experimentally characterize a new class of silicon photonic modulators—the adiabatic microring modulator. This device leverages the adiabatic microring resonator, designed to eliminate the coupling of higher-order TE optical modes to achieve uncorrupted FSRs and low insertion losses. This modulator, similar to the silicon microdisk modulator, leverages the depletion-based vertical-junction configuration, which maximizes the overlap of the depletion region with the optical mode, minimizing the power consumption. Furthermore, the silicon adiabatic microring modulator employs a unique adiabatic design that eliminates higher-order modes that are present in the silicon microdisk modulator, yielding an uncorrupted 56.12-nm (6.92-THz) FSR. Moreover, we demonstrate that the partially-doped configuration of these silicon photonic modulators reduces the resistance and enhances the speed of these devices.

We perform a detailed comparative analysis between four silicon photonic modulators, including silicon microdisk modulators and silicon adiabatic microring modulators, with full and partial doping configurations, and as well as the commercial lithium niobate modulator. Our experimental spectral characterization of the silicon photonic modulators shows that the resonance frequency shift as a function of applied modulator diode junction voltage does not have a dependency on whether we are using the silicon adiabatic microring modulators over silicon microdisk modulators, or partial doping over full doping. Our experimental high-speed temporal characterization shows that for lower data rates, the performance of all four silicon photonic modulators is comparable. As we modulate at higher data rates, the partially-doped silicon photonic devices show much better performance. Our high-speed bit-error-rate and power penalty characterizations confirm this; the partial doping causes a reduction in relative power penalty for both types of silicon photonic modulators, enabling feasible operation of both at 12.5-Gb/s data rates and beyond. Using this partial doping, the power penalty of the silicon adiabatic microring modulator, relative to the silicon microdisk modulator, is 0.92, 1.11, and 1.31 dB, for data rates of 5, 7.5, and 10 Gb/s, respectively.

All the modulators demonstrated in this work have laterally-separated P + and N + doped regions in the center of the microdisks and adiabatic microrings. However, the PN vertical junction is circular. The capacitance of the modulators is dominated by this vertical PN junction area, for both microdisk and adiabatic microring modulators. Typical capacitances for the partially- and fully-doped modulators are about 12.5 and 25 fF, respectively. These modulators also experience high-resistance contacts where the PN vertical junction is not directly contacted by P + or N + doped regions. The contact resistance increases as the junction is separated from the P + or N + doped regions. For instance, half of the circular vertical junction is not directly contacted by one type of highly-doped regions in the fully-doped modulator. Non-directly-contacted regions are wider in the adiabatic microring modulators compared to microdisk modulators, leading to higher contact resistances. Therefore, we see that the microdisk modulators exhibit better electrical performance metrics such as the speed, dynamic extinction ratio, and power penalty, compared to the adiabatic microring modulators. Partial doping also minimizes the capacitance of the modulator, since the PN vertical junction area is decreased. Therefore, partially-doped modulators exhibit higher electrical bandwidths than fully-doped modulators, since both resistance and capacitance of these devices are minimized.

The devices in this work are currently limited to about 12.5-Gb/s data rates due to the contact resistance, which is about 0.8–1 kΩ for each via and the non-directly-contacted vertical junction combined. The resistance of the microdisk modulator can be further

#177942 - $15.00 USD Received 11 Oct 2012; revised 4 Dec 2012; accepted 10 Dec 2012; published 17 Dec 2012

minimized by increasing the number of P + and N + doped regions in the center, instead of dividing into just two laterally-doped regions. The contact resistance of the adiabatic microring modulators can be minimized either by optimizing the doping concentrations of the PN devices, increasing the number of tethers, or widening the tethers that directly contact to the adiabatic portions. Decreasing the RC time constant through this optimization could enable the adiabatic microring modulator to operate at 40-Gb/s data rates and beyond.

The silicon adiabatic microring modulator combines the best of all modulator designs, yielding an uncorrupted 56.12-nm (6.92-THz) FSR that can sustain over 100 wavelength channels in WDM systems. This compact, high-speed, and low-power modulator was also fabricated using standard CMOS-compatible wafer-scale photolithography, capable of dense integration with advanced electronics, and low-cost mass-volume production.

Acknowledgments

This work was supported in part by the Defense Advanced Research Projects Agency (DARPA) Microsystems Technology Office (MTO) Photonically Optimized Embedded Microprocessors (POEM) program, under the Silicon Photonic 3D-Integrated Reduced Energy Transmission (SPIRET) project, contract 6925995. Sandia National Laboratories is a multi-program laboratory managed and operated by Sandia Corporation, a wholly owned subsidiary of Lockheed Martin Corporation, for the U.S. Department of Energy's National Nuclear Security Administration under contract DE-AC04-94AL85000.

#177942 - $15.00 USD Received 11 Oct 2012; revised 4 Dec 2012; accepted 10 Dec 2012; published 17 Dec 2012